

Double – photon exclusive processes with heavy quark – heavy antiquark pairs in high-energy Pb-Pb collisions at LHC

M. Klusek-Gawenda,^{1,*} A. Szczurek,^{1,2,†} M.V.T. Machado,^{3,‡} and V.G. Serbo^{4,§}

¹*Institute of Nuclear Physics PAN, PL-31-342 Cracow, Poland*

²*University of Rzeszów, PL-35-959 Rzeszów, Poland*

³*High Energy Physics Phenomenology Group, GFPAE IF-UFRGS
Caixa Postal 15051, CEP 91501-970, Porto Alegre, RS, Brazil*

⁴*Novosibirsk State University, Pirogova 2, 630090, Novosibirsk, Russia*

(Dated: November 4, 2010)

Abstract

The cross section for exclusive heavy quark and heavy antiquark pair ($Q\bar{Q}$) production in peripheral ultrarelativistic heavy ion collisions is calculated for the LHC energy $\sqrt{s_{NN}} = 5.5$ TeV. Here we consider only processes with photon–photon interactions and omit diffractive contributions. We present results in the impact parameter equivalent photon approximation (EPA) and compare some of them with results obtained by exact calculations of the Feynman diagrams in the momentum space. We include both $Q\bar{Q}$, $Q\bar{Q}g$ and $Q\bar{Q}q\bar{q}$ final states as well as photon single-resolved components. Realistic charge densities in nuclei were taken in the calculation. The different components give contributions of the same order of magnitude to the nuclear cross section. The cross sections found here are smaller than those for the diffractive photon-pomeron mechanism and larger than diffractive pomeron-pomeron discussed in the literature.

PACS numbers: 14.65.Fy, 14.65.Dw, 25.75.-q, 25.75.Dw, 25.20.Lj

*Electronic address: mariola.klusek@ifj.edu.pl

†Electronic address: antoni.szczurek@ifj.edu.pl

‡Electronic address: magnus@if.ufrgs.br

§Electronic address: serbo@math.nsc.ru

I. INTRODUCTION

Heavy quark – heavy antiquark production was studied in the past in photon-photon, photon-proton, inclusive and exclusive proton–proton and heavy ion collisions when the ions break apart. In principle, the heavy quark – heavy antiquark pairs can be produced also in exclusive coherent $\gamma\gamma$ processes when the nuclei stay intact. These processes, in analogy to lepton pair production [1, 2], should be “increased” by the large charges of the colliding nuclei. On the other hand the effects of the nuclear form factors which diminish contributions of large energy virtual photons should be included. Recently two of us (M.K.+A.S.) have shown [3] that the inclusion of realistic form factors (corresponding to realistic charge densities) is essential for reliable estimation of the cross sections for exclusive lepton–pair production especially for large rapidities and large transverse momenta of the produced particles. The inclusion of the realistic form factor should be even more important for heavy quark – heavy antiquark pair production.

In contrast to dileptons the $Q\bar{Q}$ state cannot be directly observed. In practice one measures rather heavy mesons or electrons from their semileptonic decays. Then the final states are already complicated due to hadronization process. Therefore one has to include also different, yet simple, partonic states as $Q\bar{Q}g$ and $Q\bar{Q}q\bar{q}$.

Recently one of us (M.M.) with coworkers made an estimation of the cross sections for diffractive mechanisms [4]. It is of interest to make a realistic estimate of the cross section for photon–photon mechanism and compare it with the diffractive contribution.

II. HEAVY QUARK – HEAVY ANTIQUARK PAIR PRODUCTION

A. Photon–photon subprocesses

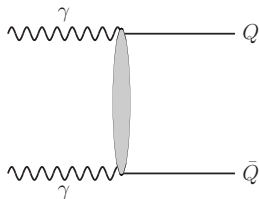


FIG. 1: Representative diagram for the Born amplitude.

In the present analysis we include the mechanisms shown in Fig. 1, 2, 3, 4. The first one (called sometimes direct) is identical as the one for the production of charged lepton pairs. In contrast to the dilepton production in the case of the quark production one has to include also QCD corrections. Corresponding diagrams for NLO approximation are shown in Fig. 2. Heavy quarks can be also produced in association with light quark-antiquark pairs as shown in Fig. 3. The last two diagrams correspond to single-resolved components when only small part of one photon interacts with the other photon. All these processes were studied in detail in Refs.[5–7].

Let us start with the Born direct contribution. The leading–order elementary cross section

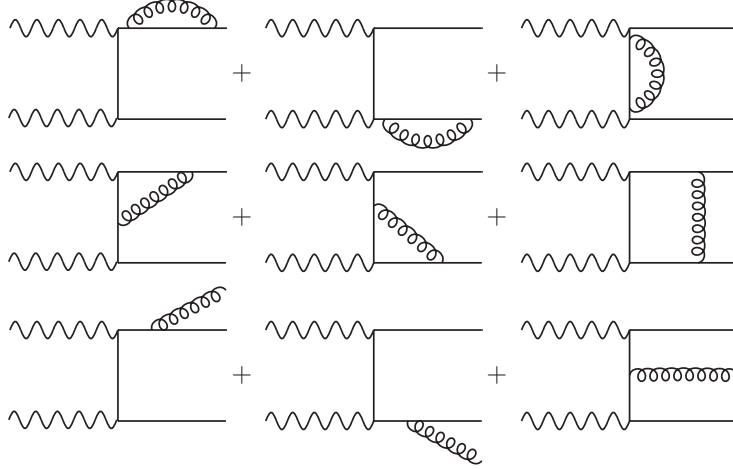


FIG. 2: Representative diagrams for the leading-order QCD corrections.



FIG. 3: Representative diagrams for $Q\bar{Q}q\bar{q}$ production.

for $\gamma\gamma \rightarrow Q\bar{Q}$ at 2-photon energy $W_{\gamma\gamma}$ takes the simple form

$$\sigma_{\gamma\gamma \rightarrow Q\bar{Q}}^{direct}(W_{\gamma\gamma}) = N_c e_Q^4 \frac{4\pi\alpha_{em}^2}{W_{\gamma\gamma}^2} \times \left\{ 2 \ln \left[\frac{W_{\gamma\gamma}}{2m_Q} (1+v) \right] \left(1 + \frac{4m_Q^2 W_{\gamma\gamma}^2 - 8m_Q^4}{W_{\gamma\gamma}^4} \right) - \left(1 + \frac{4m_Q^2 W_{\gamma\gamma}^2}{W_{\gamma\gamma}^4} \right) v \right\}, \quad (2.1)$$

where $Q\bar{Q} = c\bar{c}, b\bar{b}$, $N_c = 3$ is the number of quark colors, $v = \sqrt{1 - \frac{4m_Q^2}{W_{\gamma\gamma}^2}}$ and e_Q is the fractional charge of the heavy quark. The formula has been derived for the first time in Ref. [8]. In the current calculation we take the following heavy quark masses: $m_c = 1.5$ GeV, $m_b = 4.75$ GeV. This formula can be directly used in the impact-parameter-space (called here b -space for brevity) equivalent photon approximation (EPA), as we will see below. It is obvious that the final $Q\bar{Q}$ state cannot be observed experimentally due to the quark confinement and rather heavy mesons have to be observed instead. It is noticed that the



FIG. 4: Representative diagrams for the single-resolved mechanism.

presence of additional few light mesons is rather natural.¹ This forces one to include more complicated final states.

In contrast to QED production of lepton pairs in photon-photon collisions, in the case of $Q\bar{Q}$ production one needs to include also higher-order QCD processes which are known to be rather significant. Here we include leading-order corrections only for the dominant, in heavy-ion collisions, direct contribution. The details concerning the higher-order corrections to heavy quark and heavy antiquark production in photon-photon collisions can be found in [10–17]. In α_s -order there are one-gluon bremsstrahlung diagrams ($\gamma\gamma \rightarrow Q\bar{Q}g$) and interferences of the Born diagram with self-energy diagrams (in $\gamma\gamma \rightarrow Q\bar{Q}$) and vertex-correction diagrams (in $\gamma\gamma \rightarrow Q\bar{Q}$). The relevant diagrams are shown in Fig.2. In the present analysis we follow the approach presented in Ref. [17]. The QCD corrections can be written as

$$\sigma_{\gamma\gamma \rightarrow Q\bar{Q}(g)}^{QCD}(W_{\gamma\gamma}) = N_c e_Q^4 \frac{2\pi\alpha_{em}^2}{W_{\gamma\gamma}^2} C_F \frac{\alpha_s}{\pi} f^{(1)}. \quad (2.2)$$

The function $f^{(1)}$ is calculated using a code provided by the authors of Ref. [17] which uses program package HPL [18]. In the present analysis the scale of α_s is fixed at $\mu^2 = 4m_Q^2$.

We include also the subprocess $\gamma\gamma \rightarrow Q\bar{Q}q\bar{q}$, where q (\bar{q}) are light, u , d , s , quarks (antiquarks). The cross section for this mechanism can be easily calculated in the color dipole framework [5–7]. In the dipole–dipole approach [6] the total cross section for the $\gamma\gamma \rightarrow Q\bar{Q}$ production can be expressed as

$$\begin{aligned} \sigma_{\gamma\gamma \rightarrow Q\bar{Q}}^{4q}(W_{\gamma\gamma}) &= \sum_{f_2 \neq Q} \int \left| \Phi^{Q\bar{Q}}(\rho_1, z_1) \right|^2 \left| \Phi^{f_2\bar{f}_2}(\rho_2, z_2) \right|^2 \sigma_{dd}(\rho_1, \rho_2, x_{Qf}) d^2\rho_1 dz_1 d^2\rho_2 dz_2 \\ &+ \sum_{f_1 \neq Q} \int \left| \Phi^{f_1\bar{f}_1}(\rho_1, z_1) \right|^2 \left| \Phi^{Q\bar{Q}}(\rho_2, z_2) \right|^2 \sigma_{dd}(\rho_1, \rho_2, x_{fQ}) d^2\rho_1 dz_1 d^2\rho_2 dz_2, \end{aligned} \quad (2.3)$$

where $\Phi^{Q\bar{Q}}(\rho, z)$ are the quark – antiquark wave functions of the photon in the mixed representation and σ_{dd} is the dipole–dipole cross section. Eq.(2.3) is correct at sufficiently high energy $W_{\gamma\gamma} \gg 2m_Q$. At lower energies, the proximity of the kinematical threshold is a concern. In Ref. [5] a phenomenological saturation–model inspired parametrization for the azimuthal angle averaged dipole–dipole cross section has been proposed:

$$\sigma_{dd}^{a,b} = \sigma_0^{a,b} \left[1 - \exp\left(-\frac{r_{\text{eff}}^2}{4R_0^2(x_{ab})}\right) \right]. \quad (2.4)$$

Here, the saturation radius is defined as

$$R_0(x_{ab}) = \frac{1}{Q_0} \left(\frac{x_{ab}}{x_0} \right)^{-\lambda/2} \quad (2.5)$$

and the parameter x_{ab} which controls the energy dependence was given by

$$x_{ab} = \frac{4m_a^2 + 4m_b^2}{W_{\gamma\gamma}^2}. \quad (2.6)$$

¹ There are also final states with exclusively two $Q\bar{q}$ and $\bar{Q}q$ mesons [9]. The corresponding cross sections are however much smaller.

In the numerical calculations we are using the model parameters $(x_0, \lambda, \sigma_0, m_q)$ for an effective radius $r_{\text{eff}}^2 = (\rho_1 \rho_2)^2 / (\rho_1 + \rho_2)$ [5]. Some other parametrizations of the dipole-dipole cross section were discussed in the literature (see e.g. [19]). The cross section for the $\gamma\gamma \rightarrow Q\bar{Q}q\bar{q}$ process here is much bigger than the one corresponding to the tree-level Feynman diagram [15] as it effectively resums higher-order QCD contributions.

As discussed in Ref. [6] the $Q\bar{Q}q\bar{q}$ component have very small overlap with the single-resolved component because of quite different final state, so adding them together does not lead to double counting. The cross section for the single-resolved contribution can be written as:

$$\sigma_{1-res}(s) = \int dx_1 [g_1(x_1, \mu^2) \hat{\sigma}_{g\gamma}(\hat{s} = x_1 s)] + \int dx_2 [g_2(x_2, \mu^2) \hat{\sigma}_{\gamma g}(\hat{s} = x_2 s)], \quad (2.7)$$

where g_1 and g_2 are gluon distributions in photon 1 or photon 2 and $\hat{\sigma}_{g\gamma}$ and $\hat{\sigma}_{\gamma g}$ are elementary cross sections. In our evaluation we take the gluon distributions from Ref. [20].

In Fig. 5 we show the elementary cross sections for all processes as a function of the photon-photon center-of-mass energy. For charmed quark the direct term dominates at low energies near the threshold while the four-quark component at slightly larger energies and the resolved components at even larger energies. For bottom quarks the four-quark component is always larger than the direct term.

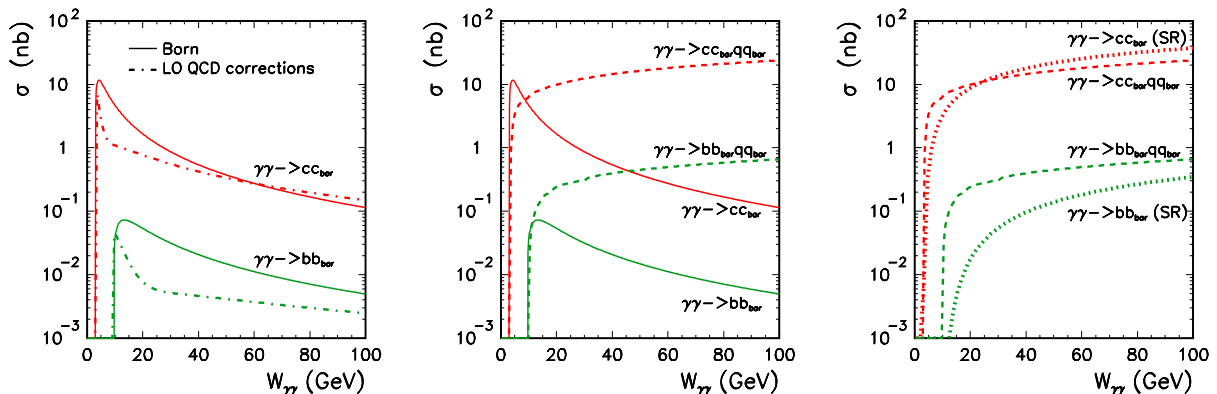


FIG. 5: The elementary cross section for the different processes as a function of the photon-photon center-of-mass energy. In the left panel we show the Born cross section (solid line) and leading-order QCD corrections (dash-dotted line). In the middle panel we show contribution of four-quark final states as calculated in the saturation model. In the right panel we show in addition contribution of single-resolved processes.

It is not clear a priori how this will change in the nucleus-nucleus collisions where one should take into account photon-photon luminosities. This will be discussed in the result section.

B. b -space EPA

Here we wish to sketch the b -space EPA used in the present analysis. The details on its development can be found in Ref. [3].

The total cross section for the $PbPb \rightarrow PbPbQ\bar{Q}$ process can be factorized into the equivalent photon spectra, $N(\omega, b)$, and the $\gamma\gamma \rightarrow Q\bar{Q}$ subprocess cross section as:

$$\begin{aligned} \sigma(PbPb \rightarrow PbPbQ\bar{Q}; s_{PbPb}) &= \int \hat{\sigma}(\gamma\gamma \rightarrow Q\bar{Q}; W_{\gamma\gamma}) \theta(|\mathbf{b}_1 - \mathbf{b}_2| - 2R_A) \\ &\times N(\omega_1, \mathbf{b}_1) N(\omega_2, \mathbf{b}_2) d^2\mathbf{b}_1 d^2\mathbf{b}_2 d\omega_1 d\omega_2. \end{aligned} \quad (2.8)$$

After performing a change of integration variables, the cross section can be expressed as the five-fold integral:

$$\begin{aligned} \sigma(PbPb \rightarrow PbPbQ\bar{Q}; s_{PbPb}) &= \int \hat{\sigma}(\gamma\gamma \rightarrow Q\bar{Q}; W_{\gamma\gamma}) \theta(|\mathbf{b}_1 - \mathbf{b}_2| - 2R_A) \\ &\times N(\omega_1, \mathbf{b}_1) N(\omega_2, \mathbf{b}_2) 2\pi b db d\bar{b}_x d\bar{b}_y \frac{W_{\gamma\gamma}}{2} dW_{\gamma\gamma} dY, \end{aligned} \quad (2.9)$$

where the quantities $\bar{b}_x \equiv (b_{1x} + b_{2x})/2$, $\bar{b}_y \equiv (b_{1y} + b_{2y})/2$ and $\mathbf{b} = \mathbf{b}_1 - \mathbf{b}_2$ have been introduced. Eq. (2.9) is used to calculate the total cross section for the $PbPb \rightarrow PbPbQ\bar{Q}$ reaction as well as the distributions in impact parameter $b = |\mathbf{b}|$, $W_{\gamma\gamma} = M_{Q\bar{Q}}$ and quark pair rapidity $Y(Q\bar{Q}) = \frac{1}{2}(y_Q + y_{\bar{Q}})$. A detailed derivation of formula (2.9) can be found in [3]. The photon flux can be expressed in terms of the charge form factors $F(Q^2)$ as:

$$N(\omega, b) = \frac{Z^2 \alpha_{em}}{\pi^2} \frac{1}{b^2 \omega} \left(\int_0^\infty u^2 J_1(u) \frac{F(Q^2)}{Q^2} du \right)^2, \quad Q^2 = \frac{\left(\frac{b\omega}{\gamma}\right)^2 + u^2}{b^2}, \quad (2.10)$$

where J_1 is the Bessel function of the first kind, $Q^2 = -q^2 > 0$ and q is the four-momentum of the quasireal photon. The form factor is the Fourier transform of the nucleus charge distribution, $\rho(r)$:

$$F(Q^2) = \int \frac{4\pi}{Q} \rho(r) \sin(Qr) r dr = 1 - \frac{Q^2 \langle r^2 \rangle}{3!} + \frac{Q^4 \langle r^4 \rangle}{5!} + \dots \quad (2.11)$$

III. RESULTS

Now we will discuss the nuclear cross sections obtained within b -space EPA described shortly above.

Let us start with the direct contribution. In Fig. 6 we show the differential distribution in photon-photon energy which for the direct component is also the distribution in the quark - antiquark invariant mass. They are presented without (dashed line) and with (solid line) absorption effects. This is done in the b -space by integrating over impact parameter either in the full range of $b > 0$ (without absorption) or for $b > R_1 + R_2$ (with absorption), where $R_{1,2}$ are the nuclei radii. For lead nucleus $R_A = 1.2 A^{1/3} \simeq 7$ fm. The results for the $c\bar{c}$ are shown on the left hand side whereas the results for the $b\bar{b}$ on the right hand side of the figure. One can clearly see that the cross section for the $c\bar{c}$ pair is considerably larger than that for the $b\bar{b}$ pair (this is because of the charge and mass differences). We will return to it when discussing total cross sections at the end of this section.

Above we have shown results obtained in the equivalent photon approximation. The same observable can be also obtained calculating Feynman diagrams in the momentum space. The details of this calculation have been carefully presented in paper [3]. In Fig. 7 we compare

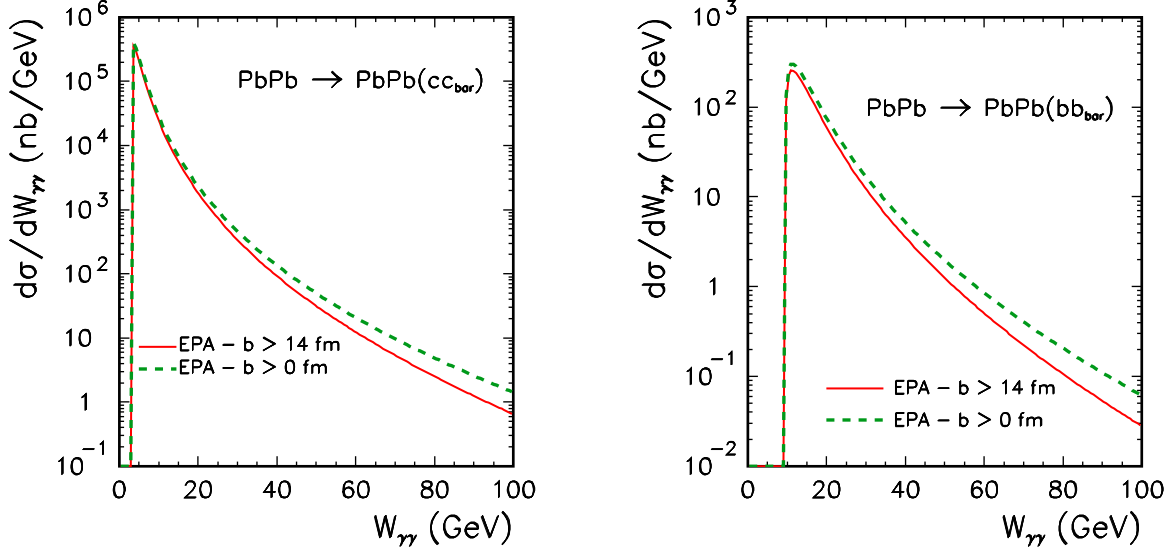


FIG. 6: The $\gamma\gamma$ subsystem energy distribution, $\frac{d\sigma}{dW_{\gamma\gamma}}$, for $PbPb \rightarrow PbPbc\bar{c}$ (left panel) and $PbPb \rightarrow PbPbb\bar{b}$ (right panel). The solid line denotes the cross section calculated within EPA approach for peripheral collisions ($b > 14$ fm) while the dashed line includes also central collisions.

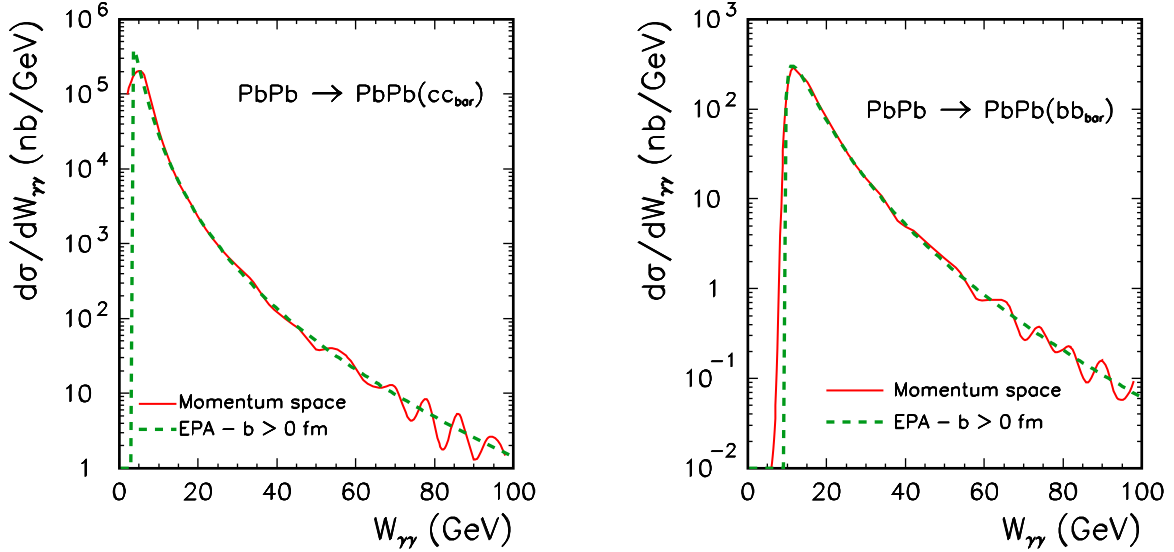


FIG. 7: The nuclear cross section as a function of $\gamma\gamma$ subsystem energy for the $PbPb \rightarrow PbPbc\bar{c}$ (left panel) and for the $PbPb \rightarrow PbPbb\bar{b}$ (right panel) reactions calculated in the EPA approximation (dashed lines) and in the momentum space (solid line).

the EPA results and those for momentum space calculation. The numerical results for the two methods are quite similar.

In Fig. 8 we compare the contributions of different mechanisms discussed in the present paper as a function of the photon–photon subsystem energy. For the Born case it is identical as a distribution in quark–antiquark invariant mass. In the other cases the photon–photon subsystem energy is clearly different than the $Q\bar{Q}$ invariant mass. Therefore, this distribution

is rather theoretical and would be difficult to measure experimentally. These distributions reflect the energy dependence of the elementary cross sections (see Fig.5). Please note a sizable contribution of the leading-order corrections close to the threshold and at large energies for the $c\bar{c}$ case. Since in this case $W_{\gamma\gamma} > M_{Q\bar{Q}}$, it becomes clear that the $Q\bar{Q}q\bar{q}$ contributions must have much steeper dependence on the $Q\bar{Q}$ invariant mass than the direct one which means that large $Q\bar{Q}$ invariant masses are produced mostly in the direct process. In contrast, small invariant masses (close to the threshold) are populated dominantly by the four-quark contribution. Therefore, measuring the invariant mass distribution one can disentangle the different mechanisms. As far as this is clear for the $c\bar{c}$ it is less transparent and more complicated for the $b\bar{b}$ production. In the last case, the experimental decomposition may be in practice not possible.

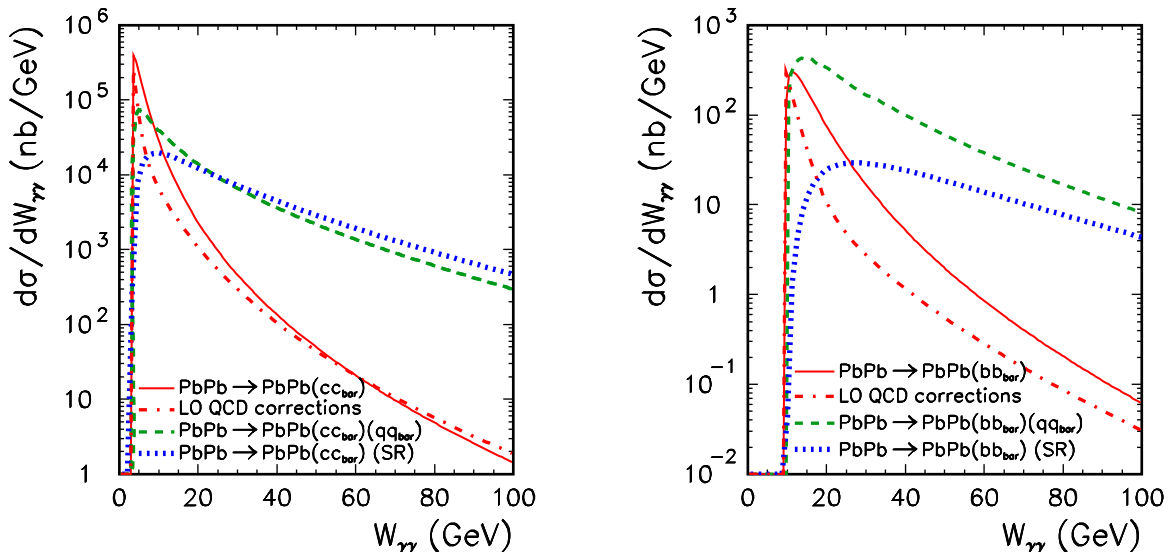


FIG. 8: The nuclear cross section as a function of photon–photon subsystem energy $W_{\gamma\gamma}$ in EPA. The red solid line denotes the results corresponding to the Born amplitude ($c\bar{c}$ -left panel and $b\bar{b}$ -right panel). The leading–order QCD corrections are shown by the red (on line) dash-dotted line. For comparison we show the differential distributions in the case when an additional pair of light quarks is produced in the final state (dashed lines) and for the single-resolved components (dotted line).

Another distribution which can be calculated in the b -space EPA is the distribution in rapidity of the particles produced in the final state: i.e. rapidity of the $Q\bar{Q}$ pair for the direct component, the rapidity of the whole $Q\bar{Q}g$ or $Q\bar{Q}q\bar{q}$ system for the $Q\bar{Q}g$ and four–quark component or the rapidity of the very complicated system for the single-resolved components. In Fig. 9 we present distributions in such a variable for all components, for $c\bar{c}$ (left panel) and $b\bar{b}$ (right panel) production. It may be quite difficult to reconstruct the $Q\bar{Q}g$ and four–quark rapidity distribution experimentally and even more difficult to reconstruct the rapidity of the complex final state for the single-resolved components. The distribution for the single-resolved components is narrower than for the other components which is related to the fact that large part of the energy is taken by the photon remnants.

Finally, in Tables 1, 2, 3 and 4 we have summarized the results for the total cross sections for different components calculated within distinct methods: b -space EPA, exact momentum

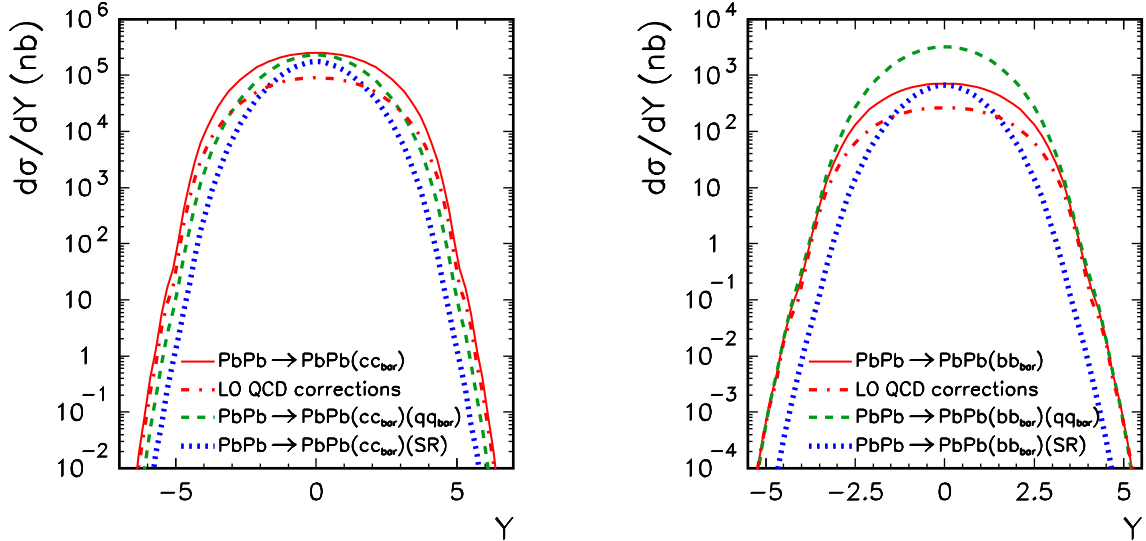


FIG. 9: The rapidity distribution, $\frac{d\sigma}{dY}$, in the b -space EPA. Here the impact parameter is in the whole range of impact parameter ($0 < b < \infty$). The red (on line) solid line denotes the results corresponding to the Born amplitude ($c\bar{c}$ -left panel and $b\bar{b}$ -right panel) and the dash-dotted line corresponds to the leading-order QCD corrections. For comparison we show the differential distributions in the case when an additional pair of light quarks is produced in the final state (dashed lines) and for the single-resolved component (dotted line).

space and momentum-space EPA described in detail in [2].

In Table 1 we present the cross sections for the Born direct component only. In order to illustrate the absorption effect we show both the integral calculated from 0 to “infinity” and the integral calculated from $R_1 + R_2$ to “infinity”. The integration in b is only slowly convergent, especially for the lighter $c\bar{c}$ pairs. Therefore we also show the practical upper limit dependence of the cross section. We are not sure that the upper limit for $c\bar{c}$ is sufficient. The results obtained within momentum-space EPA [2] are very similar to those obtained in the exact momentum space method [3]. For $b\bar{b}$ these results are also in good agreement with the b -space EPA.

In Table 2 we have ensambled leading-order QCD corrections. They constitute about one third of the Born contribution.

In Table 3 we show results for the $Q\bar{Q}q\bar{q}$ components obtained using b -space EPA. The cross sections here are of the similar order of magnitude as those for the direct component. For charm, the cross section for $Q\bar{Q}q\bar{q}$ is approximately equal to the direct contribution. On the other hand, for bottom the result is almost four times bigger than the direct component. This is due the dominance of four-quark component even near threshold as shown in Fig. 5. That feature is already known from Ref. [6], where the dipole-model was compared with LEP data for $\sigma(e^+e^- \rightarrow b\bar{b}X)$.

For completeness in Table 4 we present results for the single-resolved component. The cross sections for this component is comparable to the other components.

Finally, in Table 5 we present cross sections which include all discussed mechanisms and their relative contributions. We see that the Born mechanism dominates for $c\bar{c}$ production but four-quark component for $b\bar{b}$ production.

TABLE I: Total cross section for the $Q\bar{Q}$ component calculated within different methods.

Process	b -space EPA		Momentum- -space	Momentum- -space EPA
	$b>0$	$b>14 fm$		
$PbPb \rightarrow PbPb c\bar{c}$	$1.18 mb$ ($b<4000 fm$)	$1.05 mb$ ($b<4000 fm$)	$1.36 mb$	$1.230 mb$
	$1.13 mb$ ($b<1000 fm$)	$1.00 mb$ ($b<1000 fm$)		
$PbPb \rightarrow PbPb b\bar{b}$	$2.53 \mu b$	$2.05 \mu b$ ($b<1000 fm$)	$2.54 \mu b$	$2.54 \mu b$

TABLE II: The leading-order QCD corrections to the total cross section within b -space EPA.

Process	b -space EPA	
	$b>0$	$b>14 fm$
$PbPb \rightarrow PbPb c\bar{c}$	$0.41 mb$	$0.36 mb$
$PbPb \rightarrow PbPb b\bar{b}$	$1.00 \mu b$	$0.83 \mu b$

The event rates should be large also after hadronization process. For example, the total $c\bar{c}$ and $b\bar{b}$ two-photon rates in peripheral PbPb collisions over a 10^6 s run at LHC are $N(c\bar{c}) = 10.4 \times 10^5$ and $N(b\bar{b}) = 4.6 \times 10^3$ including Born, QCD-corrections, single-resolved and four-quark component. This is done using the b -space EPA with absorption and taking a luminosity of $\mathcal{L}_{PbPb} = 4.2 \times 10^{26} \text{ cm}^{-2}\text{s}^{-1}$. The results in Tables 1 and 4 can be compared directly to previous studies which rely on QCD collinear factorization approach, for instance in Ref. [21]. Notice that for charm the direct contribution produces similar cross sections compared to [21] whereas for bottom it is a factor two bigger. The $Q\bar{Q}q\bar{q}$ contribution was not included in [21] and in addition the single and double resolved processes were shown to be negligible for LHC energy compared to the direct one. As a short final comment, the cross sections presented in Tables 1 and 4 are larger than the estimations for the exclusive heavy-quark production in double-pomeron exchange (DPE) process (it was found in Ref. [4] $\sigma_{PbPb}^{\text{DPE}}(c\bar{c}) \approx 4.2 \mu b$ and $\sigma_{PbPb}^{\text{DPE}}(b\bar{b}) \approx 0.2 \mu b$) whereas they are smaller than the quark-pair production in photon-pomeron processes.

IV. CONCLUSIONS

In the present paper we have concentrated on production of heavy quark – heavy antiquark pairs in coherent photon–photon subprocesses. A discussion on similar diffractive processes have been already presented in the literature and will be not repeated here. The photon–photon processes are dominant in the case of exclusive production of charged lepton pairs. In our calculations we have used realistic nuclear form factors calculated as Fourier transform of the realistic charge density of the nucleus known from the electron scattering

TABLE III: Total cross section for the $Q\bar{Q}q\bar{q}$ components within b -space EPA.

Process	b -space EPA	
	$b>0$	$b>14 fm$
$PbPb \rightarrow PbPb c\bar{c}q\bar{q}$	$0.82 mb$	$0.67 mb$
$PbPb \rightarrow PbPb b\bar{b}q\bar{q}$	$9.40 \mu b$	$6.98 \mu b$

TABLE IV: Total cross section for the single-resolved components within b -space EPA.

Process	b -space EPA	
	$b > 0$	$b > 14 fm$
$PbPb \rightarrow PbPb c\bar{c}$	0.52 mb	0.39 mb
$PbPb \rightarrow PbPb b\bar{b}$	1.51 μb	0.97 μb

TABLE V: Partial contributions of different mechanisms.

	σ_{tot}	Born	QCD-corrections	4-quark	Single-resolved
$c\bar{c}$	2.47 mb	42.5 %	14.6 %	27.1 %	15.8 %
$b\bar{b}$	10.83 μb	18.9 %	7.7 %	64.5 %	8.9 %

off nuclei. Recently, this was shown to be crucial for reliable estimation of the exclusive lepton pair production.

We have calculated cross sections for exclusive production of charm–anticharm and bottom–antibottom pairs, for the $Q\bar{Q}g$ and $Q\bar{Q}q\bar{q}$ final states as well as for the single-resolved components in the high–energy peripheral lead–lead collisions for the LHC energy $\sqrt{s_{NN}} = 5.5$ GeV. Large cross sections have been found in the case of charm quarks (antiquarks) production. In contrast to the exclusive dilepton production in the case of the heavy quark - heavy antiquark production large QCD corrections appear. Their fractional contribution strongly depends on the photon-photon subsystem energy.

Two methods have been used to calculate the Born contribution: impact parameter equivalent photon approximation (b -space EPA) and the Feynman diagrammatic approach for the Born component called here momentum space approach. The b -space EPA is an approximation but allows to include absorption effects in a simple way by limiting the range of integration over impact parameter. The direct contribution was calculated in both the b -space EPA and the Feynman graph approach while the leading–order QCD correction, four–quark component as well as single-resolved components only in the b -space EPA.

We have presented total (phase space integrated) cross sections as well as some selected differential distributions relatively easy to calculate in the b -space EPA. The absorption effects turned out to be larger for bottom quarks (20 %) than for charm quarks (10 %). Since both methods lead to similar effects one can use the momentum space approach to calculate, or at least to estimate, different observables which are not straightforward in the b -space approach.

We have found that the contributions of two– and four– quark and single-resolved final states are of similar size. We have found also that the large invariant masses of the $Q\bar{Q}$ system are populated dominantly by the direct $\gamma\gamma \rightarrow Q\bar{Q}$ subprocesses while smaller invariant masses by the $\gamma\gamma \rightarrow Q\bar{Q}g$, $\gamma\gamma \rightarrow Q\bar{Q}q\bar{q}$ or single-resolved components. This could be potentially helpful in experimental identification of the all components. There are known experimental methods how to distinguish large transverse momentum b (\bar{b}) jets, therefore exclusive measurement of such jets should be possible in the LHC experiments.

The cross sections found for the QED processes discussed in the present paper seem smaller than those found in diffractive photon-pomeron processes but smaller than diffractive pomeron-pomeron process. The diffractive processes are more difficult to be reliably calculated. A combined simultaneous analysis of all processes including different differential distributions seems indispensable in the future. Since the QED processes, as demonstrated

here, can be reliably calculated it can be used as a background to the much more involved diffractive processes.

Acknowledgments

We are indebted to Zakaria Merebashvili and Oleg Veretin for providing a code which calculates QCD corrections and for a discussion of the related physics. This work was partially supported by the Polish grant N N202 078735 and N N202 249235. MTVM was supported by science funding agency CNPq, Brazil. V.G.S. is supported by of the Russian (RFBR 09-02-00263; NSh-3810.2010.2) and USA (NSF-PHY-8555454; the Missouri Research Board) grants.

-
- [1] G. Baur, K. Hencken, D. Trautmann, S. Sadovsky and Y. Kharlov, Phys. Rep. **364** (2002) 359-450.
 - [2] U. D. Jentschura and V. G. Serbo, Eur. Phys. J. **C64** (2009) 309-317.
 - [3] M. Klusek-Gawenda and A. Szczurek, Phys. Rev. **C82** (2010) 014904.
 - [4] M.B. Gay Ducati, M.M. Machado and M.V.T. Machado, arXiv:1008.4807 [hep-ph].
 - [5] N. Timneanu, J. Kwiecinski and L. Motyka, Eur. Phys. J. **C23** (2002) 513-526.
 - [6] A. Szczurek, Eur. Phys. J. **C26** (2002) 183-194.
 - [7] V.P. Gonçalves and M.V.T. Machado, Eur. Phys. J. **C29** (2003) 37.
 - [8] S.J. Brodsky, T. Kinoshita and H. Terazawa, Phys. Rev. **D4** (1971) 1532.
 - [9] M. Luszczak and A. Szczurek, a paper in preparation.
 - [10] J.H. Kühn, E. Mirkes and J. Steegborn, Z. Phys. **C57** (1993) 615.
 - [11] M. Drees, M. Krämer, J. Zunft and P.M. Zerwas, Phys. Lett. **B306** (1993) 371.
 - [12] M. Krämer and E. Laenen, Phys. Lett. **B371** (1996) 303.
 - [13] B. Kamal and Z. Merebashvili, Phys. Rev. **D58** (1998) 074005.
 - [14] S. Frixione, M. Krämer and E. Laenen, Nucl. Phys. **B57** (2000) 169.
 - [15] J. Chyla, Phys. Rev. **D70** (2004) 054001.
 - [16] J.G. Korner, Z. Merebashvili and M. Royal, Phys. Rev. **D74** (2006) 094006.
 - [17] B.A. Kniehl, A.V. Kotikov, Z.V. Merebashvili and O.L. Veretin, Phys. Rev. **D79** (2009) 114032.
 - [18] D. Maitre, Comput. Phys. Commun. **174** (2006) 222
 - [19] V.P. Gonçalves, M.S. Kugeratski, E.R. Cazaroto, F. Carvalho and F.S. Navarra, arXiv:1009.1112 [hep-ph].
 - [20] M. Gluck, E. Reya and A. Vogt, Phys. Rev. **D46** (1992) 1973.
 - [21] S. R. Klein, J. Nystrand and R. Vogt, Phys. Rev. **C66**, 044906 (2002).